SRNL-STI-2010-00399

The Stability and Electrical Properties of $Ba_{1-x}Sr_xCe_{0.8}Y_{0.2}O_{3-\delta}$ High Temperature Proton Conductors

Siwei Wang [a], Fei Zhao [a], Lingling Zhang [a], Kyle Brinkman [b], Fanglin Chen [a, *]

[a] Department of Mechanical Engineering, University of South Carolina, Columbia, SC 29208, USA

[b] Savannah River National Laboratory, Aiken, SC 29808, USA

Abstract

The morphological and electrical properties of $Ba_{1-x}Sr_xCe_{0.8}Y_{0.2}O_{3-\delta}$ with x varying from 0 to 1 prepared by a modified Pechini method were investigated as potential high temperature proton conductors. Dense microstructures were achieved for all the samples upon sintering at 1500°C for 5 h. The phase structure analysis indicated that perovskite phase was formed for $0 \leq x \leq 0.2$, while for x larger than 0.5, impurity phases of Sr_2CeO_4 and Y_2O_3 appeared. The tolerance to H_2O for the samples improved with the increase in Sr content when exposed to boiling water, while the electrical conductivity decreased from x=0 to 1. However, the resistance to CO_2 attack at elevated temperatures was not improved within the whole x range studied.

Keywords: Barium cerate; Strontium cerate; Proton conductor; Electrical conductivity; Stability

[*] Corresponding Author: (Tel.) 803-777-4875; (E-mail): chenfa@cec.sc.edu

Introduction

$SrCeO_3$ and $BaCeO_3$ based perovksite materials exhibit considerable proton conduction when doped with trivalent ions [1, 2]. $SrCeO_3$ based electrolyte materials possess predominately protonic conduction in an atmosphere containing hydrogen or steam at elevated temperatures [1], while $BaCeO_3$ based materials may exhibit mixed ionic (oxide ions and protons) conduction [3]. These high temperature proton conductors (HTPCs) can be used in applications for hydrogen gas sensors, hydrogen pumps and membranes and as electrolyte materials for intermediate temperature (500-750^{o}C) solid oxide fuel cells (SOFCs) [1, 4-6].

Many attempts have been made to improve the electrical conductivity of $SrCeO_3$ and $BaCeO_3$ based materials. Methods such as substituting isovalent and aliovalent ions into either A or B site for the ABO_3 structure [7-9] may result in modified point defect concentrations which have impact on the conductivity. In addition, materials synthesis using different preparation methods [10-12] can affect the local stoichiometry and grain boundary interfaces resulting in conductivity modifications. In certain applications, including the water gas shift reactions with gas phase carbon species present, the cerate perovskite structure isintrinsicly un-stable up to intermediate temperatures [13]. For instance, BaCeO3 is a meta-stable state and can be easily decomposed to BaO and CeO_2 [14, 15]. $SrCeO_3$ based materials also suffer from the issue of CO_2 attack to a lesser degree [15].

Kreuer *et al*. reported that it was possible to increase the lattice acidity and the chemical stability by partially replacing "B" site Ce^{4+} with more electronegative elements [16]. The introduction of Zr^{4+} ions into Ce sites to form $Ba(Ce_{1-x}Zr_x)O_{3-\delta}$ solid solution resulted in a compromise between conductivity and stability. For example, $BaZr_{0.1}Ce_{0.7}Y_{0.2}O_{3-\delta}$ has been reported to reach a conductivity of 0.03 S cm^{-1} at 700 ^{o}C in wet air while maintaining a pure phase perovskite structure under H_2 with 50 vol% H_2O at 750^{o}C for 300 h [17].

The impact of A site doping for the cerate system $BaCe_{0.9}Nd_{0.1}O_{3-\delta}$ has been investigated by Yajima *et al.* by partially substituting Ca for Ba [8]. The oxygen ion conductivity decreased with increasing Ca content although the decrease in proton conductivity was insignificant. Hung *et al*. have reported that the chemical stability could be improved by small amount of A site Sr doping on $BaCe_{0.8}Y_{0.2}O_{3-\delta}$. They reported that $Ba_{0.9}Sr_{0.1}Ce_{0.8}Y_{0.2}O_{3-\delta}$ was more stable than $BaCe_{0.7}Zr_{0.2}Y_{0.1}O_{2.95}$ when exposed to a water vapor-rich environment [18]. However, there appear to be some discrepancies with this conclusion. Regarding the stability test for the $BaCe_{0.7}Zr_{0.2}Y_{0.1}O_{2.95}$ material reported, $BaCe_{0.7}Zr_{0.2}Y_{0.1}O_{2.95}$ was treated in boiling water [19], while the $Ba_{0.9}Sr_{0.1}Ce_{0.8}Y_{0.2}O_{3-\delta}$ material reported by Hung [18] was exposed to a water vapor-rich environment at 80^{o}C. In liquid water, the kinetics of the decomposition of $BaCeO_3$ (doped or undoped) appears to be interface-controlled and is relatively fast. By contrast, in the presence of water vapor, the kinetics appears to be diffusion-controlled and relatively sluggish [20]. Therefore the different

experimental conditions utilized in literature reports on the stability of these materials have resulted in some confusion and a knowledge gap with regards to the stability of cerate perovskites under humid conditions.

This work aims to fill the knowledge gap and attempts to more completely understand the stability and the electrical properties of (Ba,Sr)$CeYO_{3-\delta}$ materials. $Ba_{1-x}Sr_xCe_{0.8}Y_{0.2}O_{3-\delta}$ (BSCY, x=0, 0.1, 0.2, 0.5, 1, denoted as BCY, BSCY1, BSCY2, BSCY5 and SCY, respectively) were prepared, the phase structure and chemical stability were investigated, and the electrical conductivities were evaluated in this work. The reactivity with water was evaluated in both liquid and gas phase conditions.

Experimental

1. Preparation

The $Ba_{1-x}Sr_xCe_{0.8}Y_{0.2}O_{3-\delta}$ powder was prepared by a modified Pechini method. Starting materials $Ba(NO_3)_2$ (Alfa Aesar, 99.95%), $Sr(NO_3)_2$ (Alfa Aesar, 99%), $Ce(NO_3)_3 \cdot 6H_2O$ (Alfa Aesar, 99.5%) and $Y(NO_3)_3 \cdot 6H_2O$ (Alfa Aesar, 99.9%) were dissolved in deionized water and the nitrate concentration of the metal ions was determined through titration. EDTA (Ethylenediaminetetraacetic acid, Alfa Aesar, 99%) and citric acid (Alfa Aesar, 99%) were used as chelating and complexing agents, to which ammonium hydroxide (Sigma-Aldrich, NH_3 content 28.0 to 30.0%) was added to promote the dissolution of EDTA in deionized water. Stoichiometric

amount of the metal precursors were then added into the chelating and complexing agents with citric acid : metal nitrates : EDTA molar ratio = 1.5 : 1 : 1.2. The solution was stirred at room temperature for 24 h, followed by heat treatment on a hot plate to obtain a brownish gel. The gel was then heated in a microwave oven to assist in foaming. Subsequently, the dried ashes were heat-treated at 600^{o}C for 4 h in air to remove organic residue, followed by calcining at 1100^{o}C for 5 h in air with a heating rate of 3^{o}C min^{-1}. The obtained powders were pulverized with 8 wt% polyvinyl alcohol (PVA) binder and pressed into pellets under 400 MPa. The green pellets were sintered at 1500^{o}C for 5 h in air.

2. Characterization

X-ray diffraction (XRD) patterns of the calcined and sintered samples were recorded on a X-ray diffractometer (Rigaku, Japan) with graphite-monochromatized CuKa radiation (λ=1.5418 Å) using a scanning rate of 5^{o} min^{-1} in the 2θ range from 20 to 80^{o}. The structure and morphology of the synthesized products were characterized by scanning electron microscopy (SEM, FEI Quanta and XL 30) equipped with an energy dispersive X-ray spectroscopy (EDS) analyzer. For stability tests, sintered samples were exposed either in boiling water or in CO_2 atmospheres. After exposure, XRD patterns of the surface of the samples were collected. For conductivity measurement, both sides of the sintered pellets were polished, painted with platinum paste, and heat-treated at 950^{o}C for 30 min prior to the electrical conductivity measurement. Platinum wires were attached to the surface of pellets. Electrical

conductivity tests were conducted using A.C impedance spectra with A.C amplitude of 10 mV on a potentiostat/galvanostat with built-in impedance analyzer (Versa STAT3-400, Princeton Applied Research) in the frequency range of 0.1 Hz to 1 MHz at the temperature range of 450-800^{o}C.

3. Results and discussion

3.1 XRD analysis

Figure 1 shows the XRD patterns of the BSCY samples sintered at 1500^{o}C for 5 h. It can be seen that a predominantly perovskite structure are formed for all the samples. However, secondary phases such as Sr_2CeO_4 and Y_2O_3 appear for higher Sr content since the solubility limit of Y in $SrCeO_3$ is less than 20% [21-22]. It is also noted that the XRD peaks splits for BCY, probably due to perovskite phase changes (orthorhombic to tetragonal). The formation of a tetragonal phase upon sintering has previously been reported in this material system [22]. With the increase in Sr content, the diffraction peaks shifted towards larger diffraction angles indicating a decrease in the lattice parameter. This can be easily understood by the fact that the radius of Sr^{2+} (1.12 Å) is smaller than that of Ba^{2+} (1.35 Å). After substituting Ba^{2+} with Sr^{2+}, the lattice parameter decreases, resulting in shift towards larger diffraction angles.

3.2 Microstructure

The microstructures of the sintered samples are shown in Fig. 2. The graphs marked with “BCY”, “BSCY1”, “BSCY2”, “BSCY5” and “SCY” are the cross-sectional images for the samples. The graph marked with “SCY Surface” is a surface image for SCY sample. It can be seen from the cross-sectional views of the samples that all the sintered samples formed dense structures. Archimedes’s water displacement measurements on the sintered disks indicate that all the sintered samples have relative densities greater than 95% of the theoretical values.

For sample BSCY5 and SCY, it is noticed that some small particles with average grain size of about 2 μm exist, indicating the formation of secondary phases. Surface morphology for sample SCY is presented in Fig. 2 and EDS patterns for selected area A (representing large grain sizes) and B (representing small grain sizes) are shown in Fig. 3 (a) and Fig. 3 (b), respectively. It is difficult to identify the highest EDS peak of Sr from that of Y in Fig. 3. However, when the relative EDS peak intensity for Sr and/or Y with Ce is compared in Fig. 3 (a) and Fig. 3 (b), it can be seen that the relative Sr and/or Y content is higher in Fig. 3 (b) (small grain sizes) than that in Fig. 3 (a) (big grain sizes). Based on the XRD result for SCY, it is reasonable to conclude that the big grains are $SrCe_{0.8}Y_{0.2}O_3$ while the small particles are either Sr_2CeO_4 or Y_2O_3. Similar results also exist in sample BSCY5. The results would suggest that the solubility of Y in $BaCeO_3$ is larger than that in $SrCeO_3$ consistent with previous observations [21-22].

3.3 Chemical stability

It has been demonstrated that $BaCeO_3$ is thermodynamically unstable in a water-containing atmosphere at elevated temperatures with the following decomposition reaction [14]

$$BaCeO_3 + H_2O \rightarrow Ba(OH)_2 + CeO_2 \quad (1)$$

Our thermodynamic calculation results on Gibbs free energy change, ΔG for reaction (1) also indicate that $BaCeO_3$ is thermodynamically unstable below 450°C (shown in Fig. 4). Some doped $BaCeO_3$ based materials, such as 20 mol% Gd-doped $BaCeO_3$, are shown to be stable in water vapor at 600 and 700°C for 1000 h but are unstable when heated in liquid water at 85°C [24]. When considering the stability test, it is thus necessary to explore the possible effect of the sample treated in water vapor at high temperature, as well as treated at low temperature. Hung *et al.* have recently reported that $Ba_{0.9}Sr_{0.1}Ce_{0.8}Y_{0.2}O_{3-\delta}$ is kinetically stable in water rich environment at 80°C. This information, however, is not definitive to conclude that $Ba_{0.9}Sr_{0.1}Ce_{0.8}Y_{0.2}O_{3-\delta}$ is stable in heated liquid water. The mechanism for $BaCeO_3$ based material to react with water can be understood in Equation (1). When $BaCeO_3$ based material is submerged in liquid water, the reaction product $Ba(OH)_2$ is soluble in water (though the solubility is modest), and the reaction product CeO_2 is insoluble, forming a porous layer on the surface of the $BaCeO_3$ based material. Water can then readily penetrate through the porous CeO_2 layer and react with the remaining $BaCeO_3$. However, in the presence of water vapor, after water reacting with a few surface monolayers of $BaCeO_3$, the

subsequent reaction would require the dissolution of H_2O into the perovskite structure via the following equation:

$$H_2O + V_O^{\cdot\cdot} + V_o^{\times} \leftrightarrow 2OH_o^{\cdot} \quad (2)$$

The proton diffusion coefficient would thus determine the rate of the dissolution of water into the perovskite lattice, which is expected to be much slower than that of the transport of liquid water through the porous layer [20]. Consequently, the two sets of data obtained by Hung [18] and Zhong [19] cannot be directly compared.

To evaluate the stability of BSCY in boiling water, sintered pellets with different contents of Sr were tested in boiling water for 4 h. Figure 5 shows the XRD patterns of the pellets after treated in boiling water. The XRD pattern of BSCY1 before exposure to boiling water was presented in Fig. 5 for comparison. It can be seen from Fig. 5 that the XRD pattern for BCY changed significantly after treatment. After boiled in water for 4 h, BCY pellet, at least on the surface of the sample, reacted with H_2O and CO_2 to form $Ba(OH)_2$, CeO_2 and $BaCO_3$, as indicated in Fig. 5. The formation of $Ba(OH)_2$ and CeO_2 can be understood by equation (1), and the formation of $BaCO_3$ may be attributed by the reaction of $BaCeO_3$ with CO_2 dissolved in water or from air. Such impurity peaks could also readily be indexed for BSCY1 and BSCY2. For BSCY5 and SCY, however, these impurity peaks are insignificant, or at least not strong enough to be indexed. In other words, for BSCY samples with higher Sr content, the stability in water is enhanced. It can also be concluded from Fig. 5 that

when placed in boiling water, $SrCe_{0.8}Y_{0.2}O_{3-\delta}$ will be more chemically stable than $BaCe_{0.8}Y_{0.2}O_{3-\delta}$.

The stability tests in carbon dioxide atmosphere at 900°C for 2 h and in wet 3vol% CO_2 (air as the balance gas, 3vol% H_2O) at 700°C for 12 h, respectively, were conducted to determine the stability of BSCY in CO_2 containing atmospheres. The XRD diffraction peaks after the CO_2 stability testing indicated that all the samples reacted with CO_2, with no observable reaction preference to either BCY or SCY. Based on chemical stability of BCY and SCY in CO_2, it is unlikely to expect that any composition of the mixture of BCY and SCY would be resistant to reactions with CO_2 at elevated temperatures.

3.4 Conductivity

Electrical conductivity data of the samples in wet H_2 in the temperature range of 450-800°C are shown in Fig. 6 (a) and (b). Figure 6 (a) shows the conductivities of BSCY measured at different temperatures as a function of Sr concentration. It can be seen that the conductivity drops with the addition of Sr^{2+} ions into the Ba sites. Given that the conductivity of doped $SrCeO_3$ is lower than that of doped $BaCeO_3$, it is not surprising that the introduction of Sr into the latter should result in a reduction in its conductivity. Furthermore secondary phases such as Sr_2CeO_4 and/or Y_2O_3 formed due to phase segregations, as presented above, would also adversely affect the total conductivity. Figure 6 (b) presents the Arrhenius plot of the conductivities as a

function of testing temperature. The activation energies of the samples are 30.28, 34.98, 44.45 and 56.0 kJ mol^{-1} for BSCY1, BSCY2, BSCY5 and SCY, respectively. There is a clear trend that the activation energy increases with the increase in Sr content. Since doped $BaCeO_3$ is oxygen deficient, in wet atmospheres, the presence of reaction (2) could lead to mixed protonic and electronic conductivity [15, 25, 26], resulting in relatively lower activation energies. Consequently, BSCY samples with more Ba content will exhibit lower activation energy. The data for $BaCe_{0.8}Y_{0.2}O_{3-\delta}$ did not show this kind of tendency. This difference may be due to the fact that $BaCe_{0.8}Y_{0.2}O_{3-\delta}$ is not as stable as BSCY in water containing atmospheres, thus leading to deterioration in conductivity when tested for extended period under high vapor pressure environment at elevated temperatures.

Conclusion

$Ba_{1-x}Sr_xCe_{0.8}Y_{0.2}O_{3-\delta}$ powders have been synthesized by using a modified Pechini method to introduce Sr into Ba sites. Phase analysis showed that Y_2O_3 and Sr_2CeO_4 existed with higher concentration of Sr content for $Ba_{1-x}Sr_xCe_{0.8}Y_{0.2}O_{3-\delta}$, indicating that the solubility of Y in $BaCeO_3$ is higher than in $SrCeO_3$. The stability tests indicated that the resistance to boiling water for $Ba_{1-x}Sr_xCe_{0.8}Y_{0.2}O_{3-\delta}$ was between that of $BaCe_{0.8}Y_{0.2}O_{3-\delta}$ and $SrCe_{0.8}Y_{0.2}O_{3-\delta}$. Contrary to the reported data, $Ba_{1-x}Sr_xCe_{0.8}Y_{0.2}O_{3-\delta}$ was less stable than $BaCe_{0.7}Zr_{0.2}Y_{0.1}O_{3-\delta}$ when exposed to boiling water. Due to the feasibility of the reaction with CO_2 for both $BaCe_{0.8}Y_{0.2}O_{3-\delta}$ and $SrCe_{0.8}Y_{0.2}O_{3-\delta}$, it was not surprising that

$Ba_{1-x}Sr_xCe_{0.8}Y_{0.2}O_{3-\delta}$ was also not stable in CO_2 containing atmospheres. The conductivity tests indicated that $Ba_{1-x}Sr_xCe_{0.8}Y_{0.2}O_{3-\delta}$ possessed the electrical conductivity between $BaCe_{0.8}Y_{0.2}O_{3-\delta}$ and $SrCe_{0.8}Y_{0.2}O_{3-\delta}$. The conductivity decreased and the activation energy increased with the increase in Sr content in $Ba_{1-x}Sr_xCe_{0.8}Y_{0.2}O_{3-\delta}$.

Acknowledgements

The authors acknowledge gratefully the financial support of the Department of Energy Nuclear Energy University Program (NEUP) (award no. 09-510) and the SRNL LDRD program.

References

[1] H. Iwahara, T. Esaka, H. Uchida, N. Maeda, Solid State Ion. 3-4 (1981) 359-363.

[2] H. Iwahara, H. Uchida, K. Ono, K. Ogaki, J. Electrochem. Soc. 135 (1988) 529-533.

[3] H. Iwahara, Solid State Ion. 52 (1992) 99-104.

[4] K.D. Kreuer, S. Adams, W. Munch, A. Fuchs, U. Klock, J. Maier, Solid State Ion. 145 (2001) 295-306.

[5] F. Zhao, R.R. Peng, C.R. Xia, Mater. Res. Bull. 43 (2008) 370-376.

[6] B.C.H. Steele, A. Heinzel, Nature 414 (2001) 345-352.

[7] F.L. Chen, O. Toft Sørensen, G.Y. Meng, D.K. Peng, J. Euro. Cera. Soc. 18 (1998) 1389-1395.

[8] T. Yajima, H. Iwahara, H. Uchida, Solid State Ion. 47 (1991) 117-124.

[9] K. Katahira, Y. Kohchi, T. Shimura, H. Iwahara, Solid State Ion. 138 (2000) 91-98.

[10] F.L. Chen, O. Toft Sørensen, G.Y. Meng and D.K. Peng, Solid State Ion. 100 (1997) 63-72.

[11] F.L. Chen, O. Toft Sørensen, G.Y. Meng and D.K. Peng, J. Thermal Anal. 49 (1997) 1255-1261.

[12] D. Ding, W. Zhu, J.F. Gao, C.R. Xia, J. Power Source 179 (2008) 177-185.

[13] C.W. Tanner, A.V. Virkar, J. Electrochem. Soc. 143 (1996) 1386-1389.

[14] N. Zakowsky, S. Williamson, J.T.S. Irvine, Solid State Ion. 176 (2005) 3019-3026.

[15] S. Gopalan, A.V. Virkar, J. Electrochem. Soc. 140 (1993) 1060-1065.

[16] K.D. Kreuer, Annu. Rev. Mater. Res. 33 (2003) 333-359.

[17] L. Yang, S.Z. Wang, K. Blinn, M.F. Liu, Z. Liu, Z. Cheng, M.L. Liu, Science 326 (2009) 126-129.

[18] I.M. Hung, H.W. Peng, S.L. Zheng, C.P. Lin, J.S. Wu, J. Power Sources 193 (2009) 155-159.

[19] Z.M. Zhong, Solid State Ion. 178 (2007) 213-220.

[20] S.V. Bhide, A.V. Virkar, J. Electrochem. Soc. 146 (1999) 2038-2044.

[21] H. Iwahara, Solid State Ion. 86-88 (1996) 9-15.

[22] P. Pasierb, M. Wierzbicka, S. Komornicki, M. Rekas, J. Power Sources 173 (2007) 681–687.

[23] N. Bonanos, K. S. Knight, B. Ellis, Solid State Ion. 79 (1995) 161-170.

[24] Z.L. Wu, M.L. Liu, J. Electrochem. Soc. 144 (1997) 2170-2175.

[25] I. Kosacki, H.L. Tuller, Solid State Ion. 80 (1995) 223-229.

[26] T. He, K.D. Kreuer, Y.M. Baikov, J. Maier, Solid State Ion. 95 (1997) 301-308.

Figure captions

Figure 1 XRD patterns of $Ba_{1-x}Sr_xCe_{0.8}Y_{0.2}O_{3-\delta}$ (BSCY, x=0, 0.1, 0.2, 0.5 and 1, denoted as BCY, BSCY1, BSCY2, BSCY5 and SCY, respectively) sintered at 1500^{o}C for 5h in air.

Figure 2 The cross-sectional views of the BSCY sample pellets and the surface view of SCY sintered at 1500^{o}C for 5h.

Figure 3 EDS patterns for selected areas in SCY Surface shown in Fig. 2: (a) EDS of area A (representing large grain sizes); (b) EDS of area B (representing small grain sizes).

Figure 4 Thermodynamic calculations on Gibbs free energy change as a function of temperature for reaction (1).

Figure 5 XRD patterns of the sintered BSCY pellets after exposure in boiling water for 4 h.

Figure 6 (a) Electrical conductivities in wet H_2 atmosphere for BSCY samples as a function of Sr concentration measured at different temperatures; (b) Arrhenius plots of the electrical conductivities for BSCY samples in wet H_2 atmosphere.

Figure 1

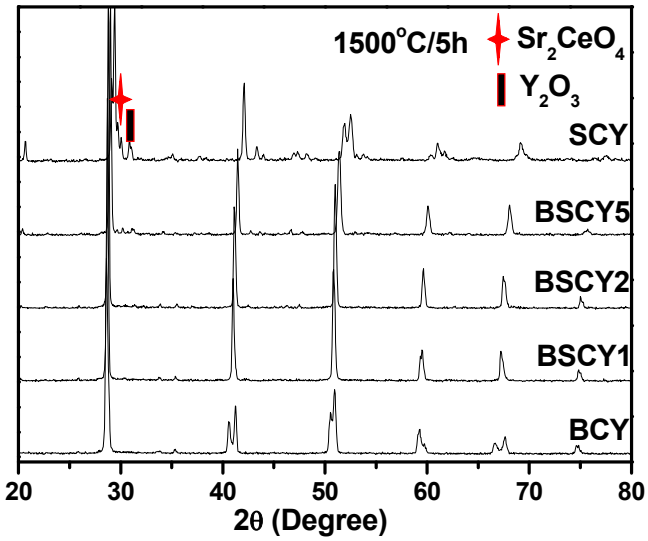
1500°C/5h
Sr2CeO4
Y2O3
SCY
BSCY5
BSCY2
BSCY1
BCY
20
30
40
50
60
70
80
2θ (Degree)

Figure 2

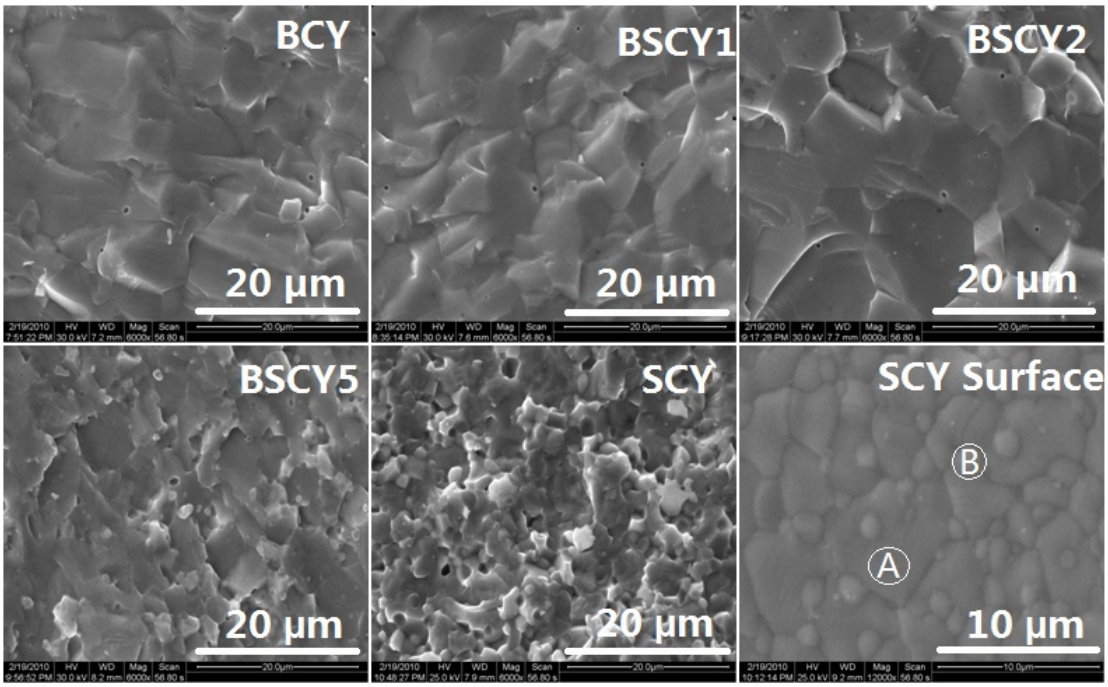
BCY
20 µm
BSCY1
20 µm
BSCY2
20 µm
BSCY5
20 µm
SCY
20 µm
SCY Surface
B
A
10 µm

Figure 3

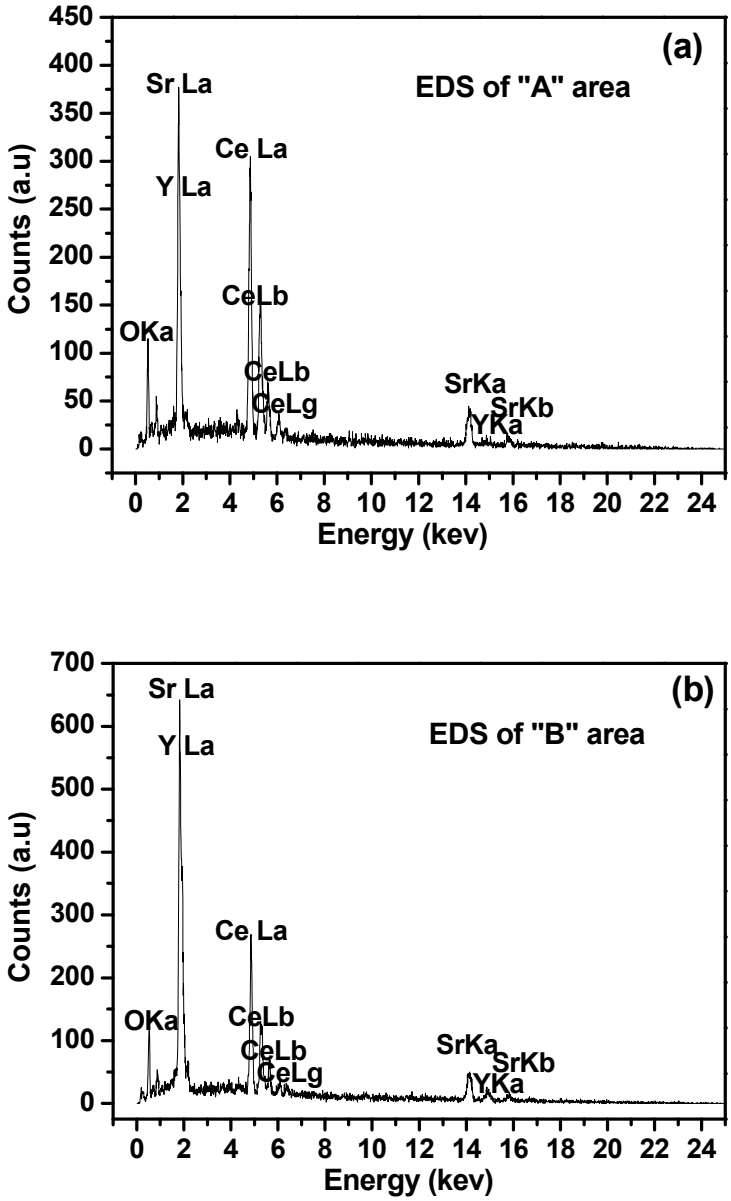
(a)
EDS of "A" area
Sr La
Ce La
Y La
CeLb
OKa
CeLb
CeLg
SrKa
SrKb
YKa
Counts (a.u)
Energy (kev)
(b)
EDS of "B" area
Sr La
Y La
Ce La
OKa
CeLb
CeLb
CeLg
SrKa
SrKb
YKa
Counts (a.u)
Energy (kev)

Figure 4

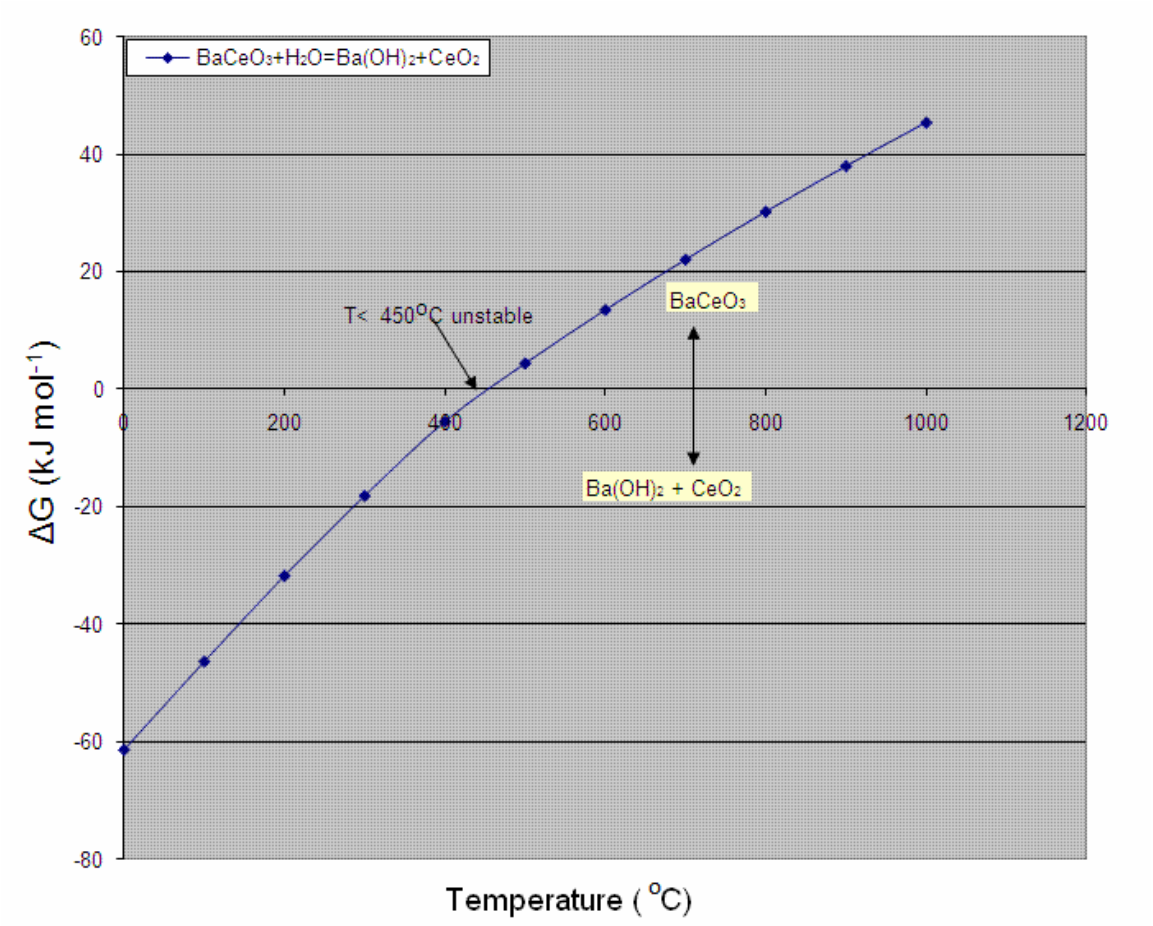
BaCeO3+H2O=Ba(OH)2+CeO2
60
40
20
0
-20
-40
-60
-80
0
200
400
600
800
1000
1200
ΔG (kJ mol-1)
Temperature (°C)
T< 450°C unstable
BaCeO3
Ba(OH)2 + CeO2

Figure 5

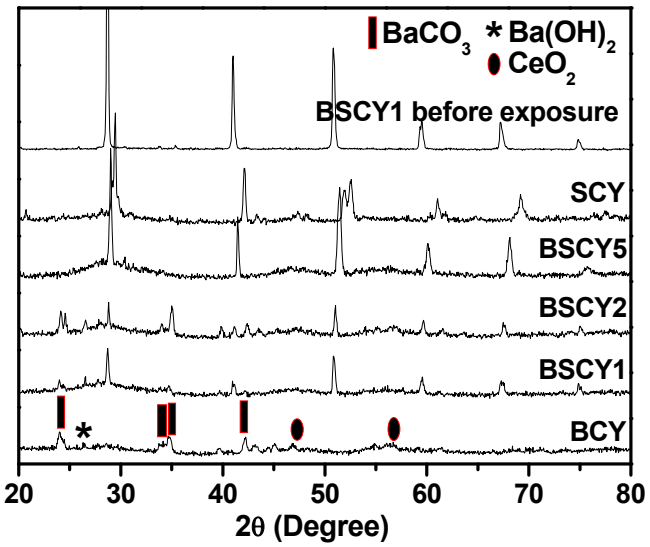
BaCO3 * Ba(OH)2
CeO2
BSCY1 before exposure
SCY
BSCY5
BSCY2
BSCY1
BCY
*
20
30
40
50
60
70
80
2θ (Degree)

Figure 6

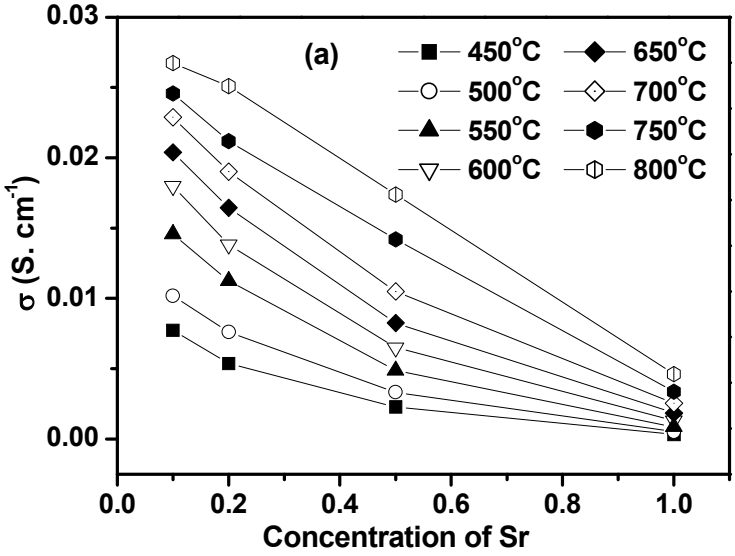
(a)
450°C
500°C
550°C
600°C
650°C
700°C
750°C
800°C
σ (S. cm-1)
Concentration of Sr
0.00
0.01
0.02
0.03
0.0
0.2
0.4
0.6
0.8
1.0

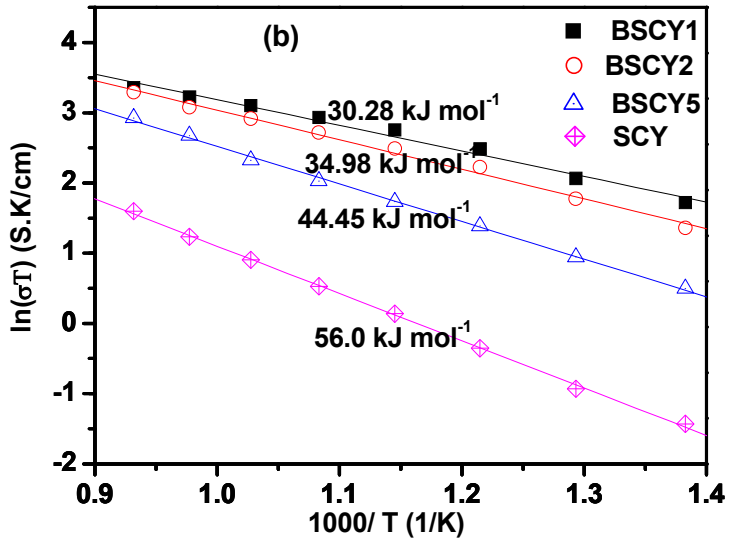
(b)
BSCY1
BSCY2
BSCY5
SCY
30.28 kJ mol-1
34.98 kJ mol-1
44.45 kJ mol-1
56.0 kJ mol-1
ln(σT) (S.K/cm)
1000/ T (1/K)
4
3
2
1
0
-1
-2
0.9
1.0
1.1
1.2
1.3
1.4